ADVANCED MATERIALS

(Fig. 4). These results explicitly indicate that Sc^{3+} ions migrated to the cathodic side, due to electrolysis, and deposited on the cathodic surface, and the mobile cationic species in $Sc_{1/3}Zr_2(PO_4)_3$ can be directly identified as Sc^{3+} ions.

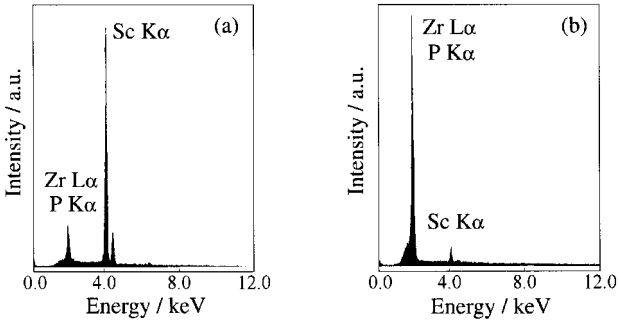

Fig. 4. The results of the EPMA spot analysis of the cathodic surface after (a) and before (b) electrolysis.

In summary, a new solid electrolyte, $Sc_{1/3}Zr_2(PO_4)_3$, was synthesized by a sol-gel method. The conducting ion species was clearly demonstrated to be the Sc^{3+} ion, and its trivalent ion conductivity was comparable to that of the $Sc_2(WO_4)_3$-type tungstate solid electrolyte series. Because the present solid electrolyte is based on phosphate containing Zr^{4+} and P^{5+}, which are extremely difficult to reduce in a variety of atmospheres, in addition to the mobile Sc^{3+} ion, the phosphate electrolyte can be applicable even in a reducing atmosphere where hexavalent tungsten ions are easily reduced. The above-mentioned properties of the Sc^{3+} ion conducting $Sc_{1/3}Zr_2(PO_4)_3$ solid electrolyte have greatly contributed to opening a new door for realizing practical applications of advanced materials such as rechargeable batteries and various types of chemical sensors.

Experimental

$Sc_{1/3}Zr_2(PO_4)_3$ was prepared by a sol-gel method using high-purity Sc_2O_3 (99.9 %), $ZrOCl_2{\cdot}8H_2O$ (99.95 %), and $NH_4H_2PO_4$ (99 %) as the starting materials. Sc_2O_3 and $ZrOCl_2{\cdot}8H_2O$ were separately dissolved in a 3 N HNO_3 solution and mixed with each other afterwards. Then a $NH_4H_2PO_4$ solution (3 %) was dropped into the mixed nitric acid solution. After white precipitation was obtained, the solution was heated at 75 °C for 24 h, then water in the solution was vaporized by heating at 130 °C for 8 h. The dried precipitate was heated at 300 °C for 24 h, and the white powder obtained was pelletized and sintered at 850 °C for 24 h. Pt electrodes were sputtered on both center surfaces of the sample pellet. The AC conductivity of the sample was measured by a complex impedance method using the Precision LCR meter (Hewlett Packard) in the frequency range between 20 Hz and 1 MHz at a temperature range of 350–600 °C in air. The polarization behavior was investigated by measuring the time dependence of the σ_{DC}/σ_{AC} ratio, and the oxygen partial pressure dependencies of the electrical conductivity were measured at oxygen pressures between 10^{-12} and 10^5 Pa. Electrolysis of the sample pellet was performed by applying a DC voltage of 3 V at 750 °C for 400 h for the purpose of identifying the conducting species, and the investigation of the cathodic surface of the sample after electrolysis was done by SEM (SEM, S-800, Hitachi) and EPMA (EPMA-1500, Shimadzu).

Received: May 31, 1999
Final version: September 20, 1999

[1] Y. Kobayashi, T. Egawa, S. Tamura, N. Imanaka, G. Adachi, *Chem. Mater.* **1997**, *9*, 1649.
[2] N. Imanaka, Y. Kobayashi, G. Adachi, *Chem. Lett.* **1995**, 433.
[3] N. Imanaka, G. Adachi, *J. Alloys Compd.* **1997**, *250*, 492.
[4] N. Imanaka, Y. Kobayashi, K. Fujiwara, T. Asano, Y. Okazaki, G. Adachi, *Chem. Mater.* **1998**, *10*, 2006.
[5] N. Imanaka, G. Adachi, *Molten Salts* **1998**, *41*, 177.
[6] N. Imanaka, Y. Kobayashi, S. Tamura, G. Adachi, *Electrochem. Solid-State Lett.* **1998**, *1*, 271.
[7] Y. Kobayashi, S. Tamura, N. Imanaka, G. Adachi, *Solid State Ionics* **1998**, *113–115*, 545.
[8] J. B. Goodenough, H. Y.-P. Hong, J. A. Kafaras, *Mater. Res. Bull.* **1976**, *11*, 203.
[9] H. Aono, N. Imanaka, G. Adachi, *Acc. Chem. Res.* **1994**, *27*, 265.
[10] M. A. Talbi, R. Brochu, C. Parent, L. Rabardel, G. L. Flem, *J. Solid State Chem.* **1994**, *110*, 350.
[11] R. D. Shannon, *Acta Crystallogr.* **1976**, *A32*, 751.

Role of Electrode Contamination in Electron Injection at Mg:Ag/Alq_3 Interfaces**

By *Chongfei Shen, Ian G. Hill,* and *Antoine Kahn**

Small-molecule organic light-emitting diodes (OLEDs) comprise interfaces formed by vacuum deposition of metals on organic materials and organic materials on metals. A typical OLED configuration includes an organic hole-transport layer deposited on a high work function anode, and a low work function cathode metal evaporated on top of an organic electron-transport layer.[1] Stacked OLEDs[2] and surface-emitting OLEDs[3] include several of these interfaces, which leads to a situation where metal-on-top and organic-on-top interfaces of a same pair of materials could operate in the same device. These interfaces, however, can have markedly different properties. Among the constituents of small-molecule OLEDs, tris (8-hydroxyquinoline) aluminum (Alq_3) is extensively used as the electron-transport and luminescent material, and Mg:Ag (weight ratio 10:1) is commonly used as the low work function (~3.7 eV) electron-injecting cathode on Alq_3. Yet, the morphology and chemistry of interfaces between these highly dissimilar materials depend sensitively on their deposition sequence. Alq_3 deposited on Mg forms a more abrupt interface than Mg deposited on Alq_3,[4,5] which reacts with the core of the molecule and diffuses into the organic layer.[5,6] New electronic states appear in the gap of the organic material at these interfaces. Similar states have been observed at interfaces between Alq_3 and Ca,[7] K and Li,[8] and Al,[6] and between PTCDA (3,4,9,10-perylenetetracarboxylic dianhy-

[*] Prof. A. Kahn, C. Shen, Dr. I. G. Hill
Department of Electrical Engineering
Princeton University
Princeton, NJ 08544 (USA)

[**] Support of this work by the Princeton MRSEC program of the National Science Foundation (Grant # DMR-9809483) and by the New Jersey Center for Optoelectronics (Grant # 97–2890-051-17) is gratefully acknowledged. The authors thank J. Schwartz, C. I. Wu, and V. Bulovic for helpful discussions, and the group of S. R. Forrest for providing purified organic materials.

  0935-9648/99/1812-1523 $ 17.50+.50/0

dride) and In, Sn, or Al.[9] The formation and occupation of these states results from a charge transfer from the metal, or metal atom, to the molecule.

The manifestation of the physical and chemical differences between metals and organic molecular solids can have direct and widespread consequences in terms of luminescence and carrier transport in OLEDs. Photoluminescence quenching near metal-on-top interfaces has been linked to the formation of non-radiative recombination centers via metal diffusion into and reaction with small-molecule and polymeric organic layers.[10,11] The situation remains a bit more confused, however, with regards to the role of reaction and interdiffusion in the carrier injection process. One previous study reported symmetric forward and backward current–voltage (I–V) characteristics for several metal/Alq_3/metal structures, including structures containing interfaces where reaction and interdiffusion are dominant.[12] Another reported highly asymmetric I–V characteristics for Mg:Ag/Alq_3/Mg:Ag structures.[13] The latter, fabricated under 10^{-5} torr vacuum, were shown to exhibit electron current injected from the metal-on-top electrode two to three orders of magnitude larger at equal voltage than the current injected from the bottom electrode. It was suggested that the asymmetry was the result of the disruption of the organic layer by the deposition of the metal, and that the injection enhancement was in part due to defects induced by the deposition of Mg at the metal-on-top interface. Although this view may hold true for some metal–organic interfaces, we show here that the environment in which the Mg:Ag/Alq_3/Mg:Ag structure is fabricated is the factor that most affects the electrical behavior of the device, and that Mg diffusion and reaction with Alq_3 have little if any effect on the charge injection. We investigate Mg:Ag/Alq_3/Mg:Ag structures fabricated and tested under high vacuum, with and without exposure of the bottom electrode to an atmosphere of nitrogen (with a substantial amount of oxygen and water vapor). We report that the chemical state of the bottom electrode surface is crucial in terms of device performance, and that the previously reported asymmetric injection behavior most likely originated from poor vacuum, leading to contamination of the bottom metal electrode during device fabrication.

All experiments were performed under an ultra-high vacuum system composed of three interconnected chambers allowing in-vacuo sample transfer between the preparation chamber, the growth chamber, and the surface analysis chamber. The samples were first loaded in the preparation chamber. The metal/organic/metal structures (Fig. 1), including the top contact, were fabricated in the growth chamber (base pressure $<2 \times 10^{-9}$ torr). The chemical analysis of the metal surfaces was performed via X-ray photoemission spectroscopy (XPS) in the analysis chamber (pressure $<1 \times 10^{-10}$ torr). The overall resolution of the XPS measurement was about 0.7 eV. I–V characterization of the diodes was performed in the preparation chamber at a base pressure of 2×10^{-8} torr in order to eliminate potential effects on the transport characteristics of cathode oxidation and deterioration of the organic layer in air.

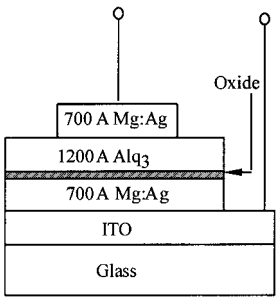

Fig. 1. Schematic diagram of the metal/Alq_3/metal structure. The shaded area represents the thin oxide layer introduced by exposure of the Mg:Ag bottom contact layer to ambient pressure.

The test structures used in this work were built on indium tin oxide (ITO)/glass substrates purchased from Applied Films Corp. The ITO cleaning procedure consisted of two consecutive five minute rinse cycles in each of boiling trichloroethylene, acetone, and boiling methanol. The surface was blown dry with high-purity nitrogen and loaded in the preparation chamber. After pumping to 2×10^{-8} torr, one of a pair of samples was transferred to the growth chamber where 700 Å Mg:Ag (10:1) followed by 1200 Å Alq_3 were deposited. A shadow mask with arrays of 0.78, 0.13, and 0.078 mm^2 round apertures was used during the deposition of the 700 Å top Mg:Ag (10:1) contact to define separate diodes. The sample was then transferred back to the preparation chamber for in-situ I–V measurements. The other sample was also transferred to the growth chamber where 700 Å Mg:Ag (10:1) was deposited and immediately transferred to the analysis chamber for XPS analysis. The O(1s), C(1s), Mg(2s), and Mg(2p) core levels were recorded using the Zr Mζ (151.4 eV) or Al Kα (1486.6 eV) photon lines of the X-ray source. The sample was then transferred back to the preparation chamber where it was subsequently exposed for ten minutes to an ambient, nitrogen-rich atmosphere (containing an unspecified amount of oxygen and water vapor). Following pumping, the sample was transferred back to the analysis chamber for XPS study, then to the growth chamber for deposition of a 1200 Å Alq_3 layer followed by 700 Å of Mg:Ag through the shadow mask for the top contact. I–V measurements were subsequently obtained in the preparation chamber.

Figure 2 shows the O(1s), Mg(2s), and Mg(2p) core level peaks measured on the Mg:Ag film before (top) and after (bottom) ambient exposure. No O(1s) is detected before exposure. The Mg(2s) and (2p) spectra excited with the Al Kα and Zr Mζ photon lines exhibit metallic peaks at 1392.7 eV and 96.9 eV, respectively. The Mg(2p) spectrum (electron escape depth = 5 Å) is considerably more surface sensitive than the Mg(2s) spectrum (electron escape depth = 20 Å). The 95.1 eV component in the Mg(2p) spectrum indicates a small amount of reacted species, presumably oxide related. The high reactivity of Mg leads to the uptake of a small fraction of a monolayer of oxygen from the resid-

  0935-9648/99/1812-1524 $ 17.50+.50/0

ADVANCED MATERIALS

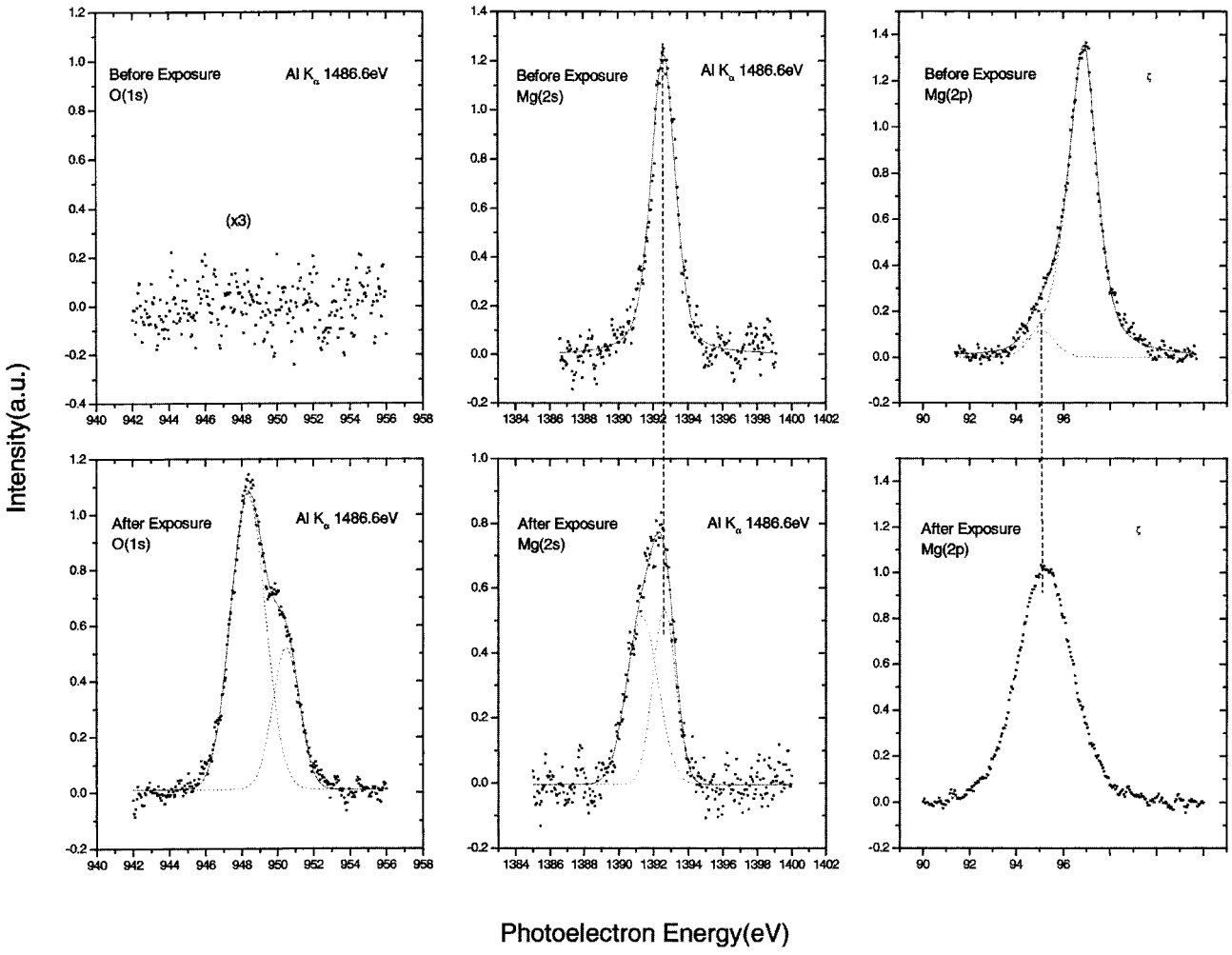

Fig. 2. O(1s) (left), Mg(2s) (middle), and Mg(2p) (right) core levels measured from the Mg:Ag bottom layer before (top) and after (bottom) exposure to an ambient nitrogen-rich atmosphere.

ual background gas during deposition or sample transfer. The photo-excitation cross-section for Mg(2p) using the Zr Mζ line is about two orders of magnitude larger than those of O(1s) and Mg(2s) using the Al Kα line, consistent with the detection of an oxide-related signal in one case and not in the others. The asymmetry on the high binding energy side of the Mg peak is also due to standard electron–electron energy loss in the process of photoemission from a metallic surface.[14]

Following ambient exposure, a large O(1s) doublet is observed. The 948.4 eV and 950 eV peaks correspond to Mg hydroxide and Mg oxide, respectively.[15,16] Both Mg(2s) and Mg(2p) core levels also exhibit new high-binding energy components. The 95.1 eV Mg(2p) component is wider than the unreacted bulk component, presumably because of multiple binding configurations in the inhomogeneous oxide layer. The metallic Mg(2s) component remains strong because the escape depth of the photoelectrons leads to a sizable contribution from the bulk Mg underneath the reacted layer. On the other hand, the metallic component of Mg(2p) is all but eliminated because of the short escape depth of the 90–100 eV electrons. A simple analysis based on peak areas of the bulk and surface-sensitive components, assuming compositional homogeneity in the reacted layer, leads to an oxide thickness of 15 ± 5 Å.

Figure 3 shows the *I–V* characteristics for the Mg:Ag/Alq_3/Mg:Ag structure without and with oxidation of the bottom electrode. Without oxidation, the electron injection currents for the top electrode negatively biased (hereafter called top-biased) and the bottom electrode negatively biased (called bottom-biased) are nearly identical (Fig. 3a). This is to be contrasted with an earlier result that reported a two orders of magnitude difference between top-biased and bottom-biased current.[13] With oxidation of the bottom electrode, however, the top-biased current becomes considerably larger than the bottom-biased current (Fig. 3b). The ratio is about two orders of magnitude above 4–5 V, reproducing closely the earlier result.[13] The top-biased current in the oxidized case is also nearly one order of magnitude smaller than in the non-oxidized case.

When the bottom electrode is not oxidized, the energy barriers for electron injection from the top and bottom

  0935-9648/99/1812-1525 $ 17.50+.50/0

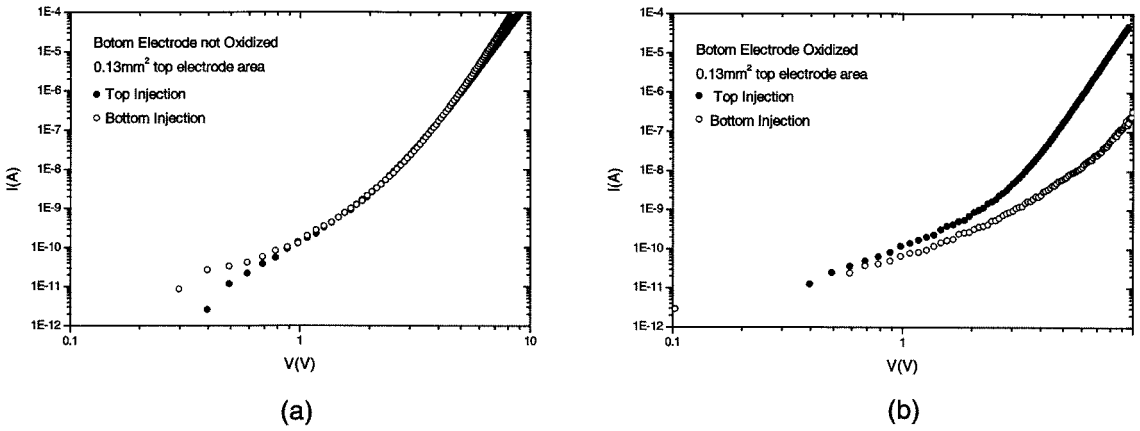

Fig. 3. Current vs. voltage characteristics for the Mg:Ag/Alq_3/Mg:Ag structure built on a) a clean and b) an oxidized bottom contact.

electrodes are about identical and 0.1 eV, according to our recent photoemission measurements.[6] This is consistent with the nearly identical top- and bottom-biased currents shown in Figure 3a.

When the bottom electrode is oxidized, the insulating Mg oxide layer affects both top- and bottom-biased currents. The top-biased injection is still determined by the 0.1 eV Mg/Alq_3 electron barrier. However, the insulating layer causes an accumulation of electrons at the bottom Alq_3/Mg interface. One consequence of this accumulation is that the electric field in Alq_3 is reduced, for the same external bias, with respect to the no-oxide case. The barrier lowering due to image force at the top Mg/Alq_3 interface is reduced, and the top-bias current decreases with respect to the no-oxide case. The most significant effect of the oxidation, however, is on the bottom-biased current for two reasons: 1) the electrons must first tunnel through the insulating layer, thus substantially reducing injection; 2) the Alq_3 highest occupied molecular orbital (HOMO) level is 0.2 eV higher with respect to the Mg Fermi level at the Alq_3/oxidized Mg interface (not shown here), thus increasing comparatively the electron-injection barrier.

The earlier report of asymmetric injection[13] was based on Mg:Ag/Alq_3/Mg:Ag structures made under moderate vacuum (10^{-5} torr). It was originally suggested that the disruption of the organic layer induced by Mg diffusion, and reaction with Alq_3 at the metal-on-top interface might help injection by providing a graded interface with a series of energy levels between the metal Fermi level and the lowest occupied molecular orbital.[4] The present experiment conclusively demonstrates that the disruption and diffusion, which are seen mainly at the Mg:Ag-on-top interface, are not the cause of the difference between top-biased and bottom-biased currents. The two orders of magnitude difference reported earlier was most likely due to an oxide layer formed on the highly reactive Mg surface in the 10^{-5} torr vacuum prior to Alq_3 deposition. The conclusion for this specific metal/organic system is therefore that the reaction and interdiffusion that take place at the metal-on-top interface are not responsible for a significant increase in efficiency of the contact, as was previously believed. The fact that the electron barrier is intrinsically small (0.1 eV) may explain why the disruption created by the metal deposition deep into the organic layer does not alter the injection. It is possible that such disruption may affect injection at larger barriers,[17] but has not yet been unambiguously established. Finally, we note that in the case where no oxide is present on the bottom electrode, the bottom-biased current is slightly larger than the top-biased current on most of the voltage range (Fig. 3a). On the other hand, Mg/Alq_3/Mg structures consistently exhibit slightly larger top-biased currents. We therefore tentatively attribute the small difference noted above to a lack of control of the Mg:Ag ratio in the top and bottom electrodes.

We investigated the effect of fabrication environment on *I–V* characteristics of nominally symmetric Mg:Ag/Alq_3/Mg:Ag structures. We showed that the structure fabricated under stringent vacuum conditions exhibits symmetric *I–V* characteristics. The results imply that the contacts formed by evaporating Mg:Ag on Alq_3, or Alq_3 on Mg:Ag, are equally efficient and that, unlike a previous report, the perturbation caused to the organic layer by the top deposited metal has no significant impact on the injection process. We further showed that the previously reported asymmetry in the *I–V* characteristics of the structure was probably due to poor vacuum, which led to the appearance of some Mg oxide during fabrication of the bottom electrode.

Received: July 5, 1999
Final version: September 17, 1999

[1] C. W. Tang, S. A. VanSlyke, *Appl. Phys. Lett.* **1987**, *51*, 913.
[2] G. Gu, V. Khalfin, S. R. Forrest, *Appl. Phys. Lett.* **1998**, *73*, 2399.
[3] V. Bulovic, P. Tian, P. E. Burrows, M. R. Gokhale, S. R. Forrest, M. E. Thompson, *Appl. Phys. Lett.* **1997**, *70*, 2954.
[4] A. Rajagopal, A. Kahn, *J. Appl. Phys.* **1998**, *84*, 355.
[5] S. T. Lee, X. Y. Hou, M. G. Mason, C. W. Tang, *Appl. Phys. Lett.* **1998**, *72*, 1593.
[6] C. Shen, J. Schwartz, A. Kahn, unpublished.
[7] V. E. Choong, M. G. Mason, C. W. Tang, Y. Gao, *Appl. Phys. Lett.* **1998**, *72*, 2689.
[8] N. Johansson, T. Osada, S. Stafström, W. R. Salaneck, V. Parente, D. A. dos Santos, X. Crispin, J. L. Brédas, *J. Chem. Phys.* **1999**, *111*, 2157.
[9] Y. Hirose, A. Kahn, V. Aristov, P. Soukiassian, V. Bulovic, S. R. Forrest, *Phys. Rev. B* **1996**, *54*, 13 748.

  0935-9648/99/1812-1526 $ 17.50+.50/0

ADVANCED MATERIALS

[10] V. E. Choong, Y. Park, Y. Gao, M. G. Mason, C. W. Tang, *J. Vac. Sci. Technol.* **1998**, *16*, 1838.
[11] V. E. Choong, Y. Park, Y. Gao, T. Wehrmeister, K. Müllen, B. R. Hsieh, C. W. Tang, *Appl. Phys. Lett.* **1996**, *69*, 1492.
[12] I. H. Campbell, D. L. Smith, *Appl. Phys. Lett.* **1999**, *74*, 561.
[13] V. Bulovic, "The Role of Excitons and Interfaces in Molecular Organic Devices", *Ph.D. Dissertation*, Princeton University **1998**.
[14] M. Cardona, L. Ley, in *Photoemission in Solids*, Springer, Berlin **1978**.
[15] J. C. Fuggle, L. M. Watson, D. J. Fabian, *Surf. Sci.* **1975**, *49*, 61.
[16] J. C. Fuggle, *Surf. Sci.* **1977**, *69*, 581.
[17] G. Parthasarathy, P. E. Burrows, V. Khalfin, V. G. Kozlov, S. R. Forrest, *J. Appl. Phys.* **1998**, *72*, 2138.

Synthesis, Structures, and Properties of New Organic Conductors Based on Tellurocycle-Fused TTF Donor Molecules

By *Emiko Ojima, Hideki Fujiwara, Hayao Kobayashi,** and *Akiko Kobayashi*

The advance of organic conductors has been accelerated by the emergence of novel molecular systems. In the search for excellent electron donors for organic conductors, interest in tellurium-containing tetrathiafulvalene (TTF) derivatives has grown over the last few years because a new metallic system with wide bandwidth and high dimensionality is expected due to the large electron cloud of tellurium atoms.[1] In addition, conducting salts based on tellurium-containing donor molecules are interesting because the tellurium network is a dominant factor in the arrangement of the whole crystal structure.[2] For example, the investigation of tellurium-substituted TTFs has been performed on tetrakis(alkyltelluro)- and (phenyltelluro)-TTFs (**1**[3] and **2**[4]) and yielded the discovery of tetrakis(methyltelluro)-TTF (**1**, $n = 1$) as a high-mobility single-component organic semiconductor owing to the two-dimensional tellurium network.[5] Recently the propyleneditelluro-substituted TTF derivatives **3**–**6** have been reported as the first examples of tellurocycle-fused TTF donor molecules.[6] Several studies have been made on their 7,7,8,8-tetracyanoquinodimethane (TCNQ) and 2,5-difluoro-TCNQ ($TCNQF_2$) complexes; however, no cation radical salt has been reported. Therefore we focused on other tellurocycle-fused TTF donor molecules. In this communication we report the synthesis, crystal structure, and electrochemical properties of a new tellurocycle-fused TTF donor, 4,5-dimethyl-4′,5′-propyleneditelluro-TTF (**7**), and crystal structures and electrical properties of the charge-transfer complex and cation radical salts prepared from **7**.

[*] Prof. H. Kobayashi, E. Ojima, Dr. H. Fujiwara
Institute for Molecular Science
Myodaiji, Okazaki 444-8585 (Japan)
Prof. A. Kobayashi
Department of Chemistry
School of Science
The University of Tokyo
Hongo, Bunkyo-ku, Tokyo 113-0033 (Japan)

The tellurocycle-fused TTF donor **7** was synthesized as shown in Scheme 1. Lithiation of dimethyl-TTF (DMTTF)[7] with lithium diisopropylamide (LDA), followed by treatment with elemental tellurium generated dilithium 4,5-dimethyl-TTF-4′,5′-ditellurolate, which was then reacted with 1,3-dibromopropane. The donor **7** was obtained as air-stable red–brown crystals in 8 % yield.

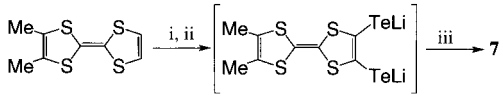

Scheme 1. Synthesis of **7**. Reagents and conditions: i) LDA (2.2 equiv.), dry THF, –78 °C, 2.5 h; ii) Te (2.0 equiv.), –78 to 0 °C, 6 h; iii) $Br(CH_2)_3Br$ (1.0 equiv.), –78 °C to room temperature, overnight.

X-ray crystallographic analysis was performed on a single crystal of **7** recrystallized from carbon disulfide/*n*-heptane. There are five crystallographically independent donor molecules, and five periodic sigmoidal stackings are formed along the *c*-axis. The TTF moieties have a bent structure resembling the molecular structure of neutral bis(ethylenedithio)-TTF (BEDT-TTF)[8] and the propyleneditelluro groups adopt a chair conformation (Fig. 1).

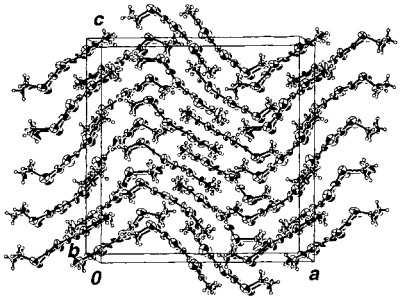

Fig. 1. The crystal structure of neutral molecule **7** viewed along the molecular short axis.

The electrochemical properties of **7** were investigated by cyclic voltammetry. The cyclic voltammogram was measured in PhCN containing tetra-*n*-butylammonium perchlorate at 20 °C. The donor molecule **7** showed three pairs of reversible redox waves at +0.37, +0.76, and +0.88 V vs. Ag/AgCl (inset of Fig. 2). On the other hand, DMTTF showed two pairs of reversible redox waves (+0.34 and +0.76 V) under identical conditions. The first and second redox potentials of **7** correspond to those of DMTTF but the first redox potential of **7** is slightly higher compared to that of DMTTF. This result suggests that the electron-donating ability of **7** is lower than that of DMTTF because of the propyleneditelluro substituent. The third redox process at +0.88 V occurs at the tellurium atoms. Similar multi-redox voltammograms have been observed for the earlier reported tellurocycle-fused TTF donors (**3**–**6**).[6] When we repeated sweeping cycles between 0.0 V and 1.2 V, all three redox waves of **7** did not change at all. However, repeated cycling between 0.0 V and 1.5 V (higher than a shoulder peak around 1.4 V) gradually extinguished only the third redox wave, which completely disappeared after 20 cycles

  0935-9648/99/1812-1527 $ 17.50+.50/0